Theory of coherent generation and detection of THz acoustic phonons using optical microcavities

N. D. Lanzillotti-Kimura,[1,*] A. Fainstein,[1] B. Perrin,[2] and B. Jusserand[2]

[1]*Centro Atómico Bariloche & Instituto Balseiro, CNEA, R8402AGP S.C. de Bariloche, Río Negro, Argentina*

[2]*Institut des NanoSciences de Paris, UMR 7588 CNRS-Université Pierre et Marie Curie, F-75004 Paris, France*

(Received 7 June 2011; revised manuscript received 13 July 2011; published 30 August 2011)

The coherent generation and detection of acoustic phonons in a superlattice embedded in an optical microcavity is theoretically analyzed. In this optical resonator, femtosecond light pulses can be spatially confined and amplified. We show that the acoustic phonon generation is enhanced as the intensity of the incident electromagnetic field is amplified in resonance with the optical microcavity. The detection process is also enhanced by the optical resonator. In the case of real photoelastic constants the maximum sensitivity occurs when the probe wavelength is tuned to where the derivative of the reflectivity has its maxima, at the optical cavity mode edges. We also analyze the role of the imaginary part of the photoelastic constants of the structure in the generation and detection processes. Finally, we study the enhancement efficiency of the microcavities when the coherent generation and detection are optimized simultaneously; we estimate phonon signals up to six orders of magnitude higher than the ones obtained with the superlattice without optical confinement.

DOI: 10.1103/PhysRevB.84.064307 PACS number(s): 78.67.Pt, 63.22.Np, 78.20.hb, 78.20.hc

I. MOTIVATION

Acoustic phonon engineering in planar nanostructures has developed great interest in recent years[1] because of its potential to improve the performance of electronic and optoelectronic devices and the perspectives of studying novel physical phenomena. Devices like phonon mirrors, cavities, filters, and structures capable of mimicking phonon potentials are a few examples of novel devices to manipulate ultrahigh-frequency acoustic phonons.[1–8] The conception of structures where light, strain, and charge can be tailored in the nanoscale[9–16] results of particular technological interest. Acoustic phonon dynamics in these nanostructures have been studied using experimental techniques in the spectral domain, such as Raman scattering, and in the time domain, such as picosecond ultrasonics.[5,16–19] One of the main concerns in the design of novel applications using acoustic phonons is the typically low signals obtained in these experiments. To overcome this limitation in Raman scattering (incoherent phonon generation), optical microcavities have been used to reach signal enhancements of up to 10^7 (Refs. 16,21–23). Raman scattering and picosecond ultrasonics (coherent acoustic phonon generation) are subject to similar selection rules. The use of microcavities in picosecond ultrasonics, although a stimulating challenge due to the prospect of realizing a coherent monochromatic source of ultrahigh-frequency acoustic phonons, has only recently been introduced and become a subject of study.[9,24,25] In this work we focus our attention on the theoretical analysis of the coherent generation and detection of acoustic phonons using optical monolithic microcavities. Particularly, we analyze how an optical microcavity enhances these coherent processes in a nanometric superlattice. This superlattice acts as the coherent generator and detector of high-frequency acoustic phonons,[26] while the optical microcavity amplifies and confines the electric field in the structure.[9]

Planar optical microcavities have been used to study the modification of photonic lifetimes,[28] parametric oscillations,[29] Bose-Einstein condensation of cavity polaritons,[30,31] polariton lasers,[32,33] and the amplification of Raman signals,[21–23] just to name a few. In this work we theoretically analyze the influence of the photon confinement in the coherent phonon generation and detection. Ultrahigh-frequency coherent phonon generation and detection has become a powerful tool in the development and study of acoustic nanodevices with novel functionalities.[3,5,10,18,26,34,35] In bulk materials, superlattices, and other nanometric multilayers the selection rules for the generation of coherent acoustic phonons are different from the ones determining their detection; this implies that the efficiency to detect the generated phonons results decreased. Optical microcavities fundamentally modify the electric field distribution in the nanostructures and thus the selection rules for both processes in such a way that the generation spectrum exactly matches the detection spectrum. In this work we show that the maximum enhancement for these processes occurs at different wavelengths and we describe in detail the experimental conditions that optimize each one of them. We focus our attention on the signal enhancement and the modification of the selection rules. We discuss the double optical enhancement (DOE) conditions under which these maximum enhancements can be reached simultaneously and analyze the efficiency and enhancement factors achievable with monolithic microcavities. Our results have potential applications in the characterization of nanostructures and novel materials and in the development of coherent and intense hypersound sources for phonon lasers.[10,36,37]

The article is organized as follows: Sec. II introduces the characteristics of the studied sample. The analysis of the coherent phonon generation is presented in Sec. III. Section IV is devoted to the detection of coherent acoustic phonons. The modification of the selection rules as a function of the detuning between the laser and the microcavity mode is studied in Sec. V. Section VI presents an analysis of the DOE, where simultaneous amplification of the generation and detection can be achieved. Finally, in Sec. VII we present a discussion of the results and the conclusions.

II. SAMPLE DESIGN

Planar optical microcavities consist of two optical distributed Bragg reflectors (DBRs) and have been extensively used in Raman scattering to amplify signals.[27] High finesse microcavities are desired to get higher electromagnetic fields. In pump-probe coherent phonon generation ultrashort laser pulses are necessary,[9] in opposition to Raman scattering where cw lasers are used. Typically, the laser pulse duration (τ_L) must be shorter than half an oscillation period of the excited acoustic phonons ($\tau_{ph}/2 = \pi/\omega_{ph}$), in order to allow impulsive generation. Here ω_{ph} is the angular frequency of the studied phonons. In an optical microcavity, due to the light confinement, another magnitude becomes relevant: the photonic lifetime (τ_{cav}). In this case, the condition for the coherent phonon generation is

$$\tau_{ph}/2 \geqslant \tau_L \geqslant \tau_{\text{cav}}. \tag{1}$$

The optical lifetime τ_{cav} is related to the finesse of the microcavity (F) by

$$\tau_{\text{cav}} = \frac{n_c L_{\text{eff}}}{c(1-R)} = \frac{F}{\omega}, \tag{2}$$

where n_c, L_{eff}, c, and R are the index of refraction and effective length of the cavity spacer (given by the actual thickness plus the penetration depth into the DBRs), the speed of light, and the optical reflectivity of the mirrors, respectively.[29] Thus, in coherent generation experiments, the finesse of the cavity results limited by the highest frequency of the studied phonons (ω_{ph}). It must be noted that if the condition $\tau_L \geqslant \tau_{\text{cav}}$ is not fulfilled, then the laser bandwidth will be filtered by the microcavity mode, and the pulse duration modified. In addition, the dependence of the microcavity response as a function of the laser wavelength would be masked by averaging effects. In other words, a finite duration of the laser pulse must be considered to allow impulsive phonon generation and detection. In what follows, we assume the spectral width of the laser pulse to be smaller than the cavity mode width, thus neglecting the laser pulse duration. We point out, however, that in a real sample design the relations between the phonon frequency, available laser pulse duration, and microcavity finesse must be taken into account.

In this work we analyze the coherent generation and detection of THz phonons in an optical microcavity. A schematic of the studied sample is shown in Fig. 1. The top (bottom) DBR is composed of 7 (10) periods of $Ga_{0.8}Al_{0.2}As$/AlAs 61.95/71.79 nm, corresponding to a ($\lambda_l/4$, $\lambda_l/4$) sequence. Here λ_l is the resonant wavelength of the microcavity. The asymmetry in the number of periods in the top and bottom DBRs is to compensate for the different reflectivities of the air/sample and sample/substrate interfaces. The optical mirrors enclose a superlattice (SL) formed by 24.5 GaAs/AlAs periods of 7.24/2.86 nm, respectively. The full SL constitutes a λ_l spacer of the optical microcavity. The thickness of the layers forming this spacer corresponds to a ($3\lambda_s/4$, $\lambda_s/4$) GaAs/AlAs SL. Here λ_s is the phonon wavelength in each material,

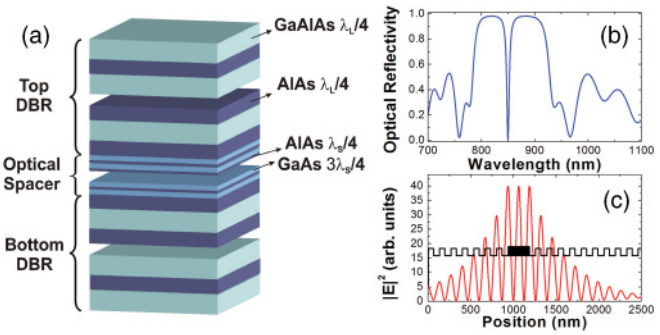

FIG. 1. (Color online) Planar optical microcavity. (a) Schematic of the sample. Two optical distributed Bragg reflectors enclose a superlattice acting as an optical spacer. (b) Calculated optical reflectivity of the microcavity. The stop band extends from 800 to 900 nm. A discrete mode can be observed at 850 nm. (c) Electric field intensity distribution calculated for a wavelength $\lambda = 850$ nm, in resonance with the optical cavity mode. The energy is localized in the spacer of the optical microcavity. An index of refraction profile is also included to facilitate the identification of the different materials. The black region corresponds to the superlattice.

corresponding to a frequency of 0.5 THz. This thickness relation optimizes the width of the first minigap at the Brillouin zone center.[17] Due to confinement effects, the electronic transitions of the quantum wells result modified. In this work we neglect excitonic resonances in the simulations.

The computation of the optical and acoustic reflectivities and electric and strain fields was performed using standard transfer matrix methods, taking into account the appropriate boundary conditions.[8] Standard values for the elastic, photoelastic, and dielectric constants were used.[38] In Fig. 1(b) we show the calculated optical reflectivity of the microcavity. Between 800 and 900 nm the stop band can be identified. The optical mode is located at 850 nm and presents a full width at half maximum of 5.4 nm. The electric field intensity for a monochromatic wave tuned with the microcavity mode is shown in Fig. 1(c); it presents an amplification of $\sim 40\times$ with respect to the field impinging on a GaAs bare substrate. The finesse of the resonator ($\lambda/\Delta\lambda$) is ~ 160. An index of refraction profile is also included in the plot to facilitate the identification of the different materials. The black region corresponds to the superlattice that acts as the cavity spacer and as the coherent phonon generator and detector of the structure.

III. COHERENT PHONON GENERATION

In this section we address the coherent acoustic phonon generation in the optical resonator. To simulate the generation process we consider a pure photoelastic mechanism only operative at the SL. This approximation relies on the following assumptions: (i) The optical microcavity mode falls in the transparency region of the SL, but close to the excitonic resonance;[15] and (ii) the photoelastic constants of the materials forming the DBRs are negligible since the gaps are well above the laser energy. Using this approach, the amplitude (g) of the

generated phononic displacement of frequency ω is calculated as[18,20]

$$g(\omega) = \int p(z)\eta(\omega,z)|E(\lambda,z)|^2 dz, \tag{3}$$

where z is the growth axis, p the photoelastic constant, η the acoustic strain, E the laser electric field, and λ the laser wavelength.

We first analyze the simple test case of a bare superlattice on a GaAs substrate [Figs. 2(c) and 2(d)], and then we study the case where the laser electric field is determined by the optical confinement of the microcavity [Figs. 2(e) and 2(f)]. In the case of a simple superlattice grown on a GaAs substrate, the modulus of the electric field is characterized by an exponentially decaying function, where the decay constant is related to the optical absorption. The spectrum calculated using Eq. (3) is shown in Fig. 2(c). The acoustic reflectivity (considering the superlattice embedded in a GaAs medium) is shown in Fig. 2(a) to identify the relevant energies. In panel (c), an intense peak at ≈500 GHz (labeled FS) is the most relevant feature of the spectrum, and corresponds to phonons with wave vector $q = 0$. These phonons are Raman active

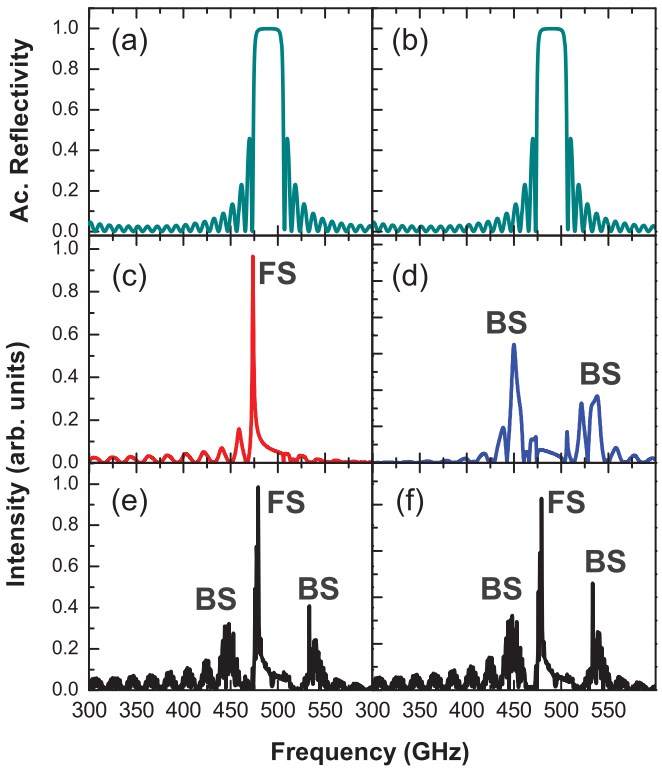

FIG. 2. (Color online) Coherent phonon generation (left column) and detection (right column). Panel (c) [(d)] Simulated coherent phonon generation [detection] spectrum in a GaAs/AlAs superlattice on a GaAs substrate. Panel (e) [(f)] Simulated coherent phonon generation [detection] spectrum in a GaAs/AlAs superlattice embedded in an optical microcavity, with the laser tuned with the optical microcavity mode (edge of the optical microcavity mode). Panels (a) and (b) show the simulated acoustic reflectivity to facilitate the identification of the modes. BS and FS indicate acoustic modes observed under backscattering and forward-scattering geometries in Raman experiments.

under forward-scattering geometry.[7,15] Neglecting the optical absorption, the electric field square modulus can be described as a constant and $p(z)$ as a material dependent value. In that case, Eq. (3) can be reduced to

$$g(\omega) \propto \int p(z)\eta(\omega,z)dz. \tag{4}$$

This expression will be maximum when $\eta(\omega,z)$ presents a periodicity identical to that of $p(z)$ (i.e., for zone-center acoustic phonons). When the superlattice is embedded in the optical microcavity, the generation spectrum is essentially different [Fig. 2(e)]. In our simulations the optical DBRs do not actively participate in the light-matter interaction; that is, we associate a null photoelastic constant to the mirrors, but only through the spatial dependence of the laser electric field in the optical spacer. The spectrum is characterized by three peaks. The so-called FS peak, and two lateral peaks related to extended vibrations in the superlattice [labeled BS in Fig. 2(e)]. To understand the origin of this modification it is necessary to consider that, under optical resonance conditions, the electric field in the spacer can be expressed as a stationary wave of the form $A(e^{ikz} + e^{-ikz})$, where k is the light wave vector and A the amplitude. In this case, Eq. (3) takes the following form:

$$g(\omega) = |A|^2 \int p(z)\eta(\omega,z)[1 + \cos(2kz)]dz, \tag{5}$$

which can be reformulated as

$$g(\omega) = |A|^2 \int p(z)\eta(\omega,z)dz + |A|^2 \int p(z)\eta(\omega,z)\cos(2kz)dz. \tag{6}$$

The first term is identical to Eq. (4), while the second term gives a finite contribution when $q = 2k$, resulting in two modes. These modes are Raman active in backscattering geometry. Thus, it can be seen that the optical microcavity changes the selection rules for the generation process. In what follows we analyze how the microcavity enhances the generation of coherent acoustic phonons.

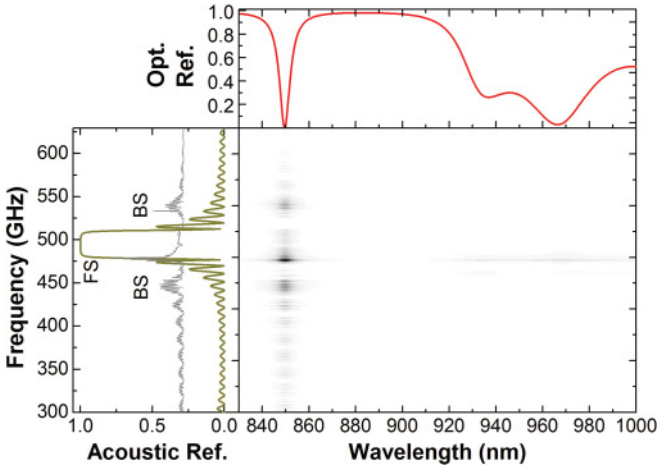

FIG. 3. (Color online) Calculated amplitude of the coherent generation spectrum as a function of the laser wavelength and the acoustic phonon frequency. (Top) Optical reflectivity of the sample. (Left) Acoustic reflectivity (thick line) and generation spectrum (gray thin line) calculated with a laser wavelength $\lambda = 850$ nm.

Figure 3 shows an intensity plot of the generation spectrum as a function of the optical wavelength and the phonon energy calculated using Eq. (3). Darker regions indicate higher phonon intensities. In the top panel we show the optical reflectivity of the structure where the confined mode can be identified at 850 nm. A high-reflectivity band can be observed between 860 and 920 nm. Note that the optical reflectivity is symmetric with respect to the center of the cavity mode. In the left panel we show the acoustic reflectivity calculated considering the superlattice embedded in a GaAs infinite medium. For clarity reasons we include in the same panel the calculated generated spectrum under the optical resonance condition from Fig. 2(e) ($\lambda = 850$ nm). From this figure it must be noted that (i) the maximum of the generated signal is achieved when the laser is tuned with the cavity mode; (ii) the generated spectrum consists of Brillouin zone center excitations ($q = 0$ at 0.48 THz, indicated as FS in the figure) and peaks related with $q \sim 2k$ at 0.45 and 0.53 THz (indicated as BS in the figure); (iii) in the high-reflectivity band the generation intensity is negligible; and (iv) between 920 and 1000 nm outside the stop band, where the optical reflectivity presents strong variations with the wavelengths, there are oscillations in the intensity and in the generated phononic bands. These oscillations are originated by the phase matching between the strain distribution, photoelastic profile, and electromagnetic field inside the spacer. The latter is neither a plane wave nor a stationary wave; thus, the generated spectrum is not a single FS peak nor a triplet of two BS and one FS peaks. It is worth noting that the maximum signal for the three main peaks is obtained exactly when the laser is tuned with the optical microcavity mode.

From Eq. (5), it can be noted that under optical resonance conditions the intensity of the signal is proportional to the maximum intensity of the electric field inside the cavity spacer ($|A^2|$). In Fig. 4 we plot the optical reflectivity [panels (a) and (b)], $|E|^2$ at the center of the microcavity spacer [panels (c) and (d)], and the amplitude of the generated FS peak [panels (e) and (f), black curve] as a function of the laser wavelength considering p_{GaAs} real. We also include in gray the amplitude of the generated FS peak considering $p_{GaAs} = i$, where i is the imaginary unit. Panels (b), (d), and (f) show a zoom around the optical microcavity mode. Several features must be marked from this plot: (i) $|E|^2$ and the FS signal present a maximum at the microcavity mode center; (ii) in the region of the stop band, included the cavity mode, the FS amplitude mimics the behavior of $|E|^2$; (iii) in the stop band edge the FS signal presents oscillations that are similar to but do not follow exactly $|E|^2$; and (iv) the generated intensity of the FS mode is independent of the nature (real or imaginary) of the photoelastic constant. To sum up, the best condition for the generation of coherent acoustic phonons (both BS and FS) is achieved when the laser is tuned with the optical microcavity, regardless of the ratio of the real/imaginary parts of the photoelastic constants.

The coherent phonon generation is qualitatively different from the coherent detection process. In the next section we will analyze in detail the detection of acoustic phonons using an optical microcavity.

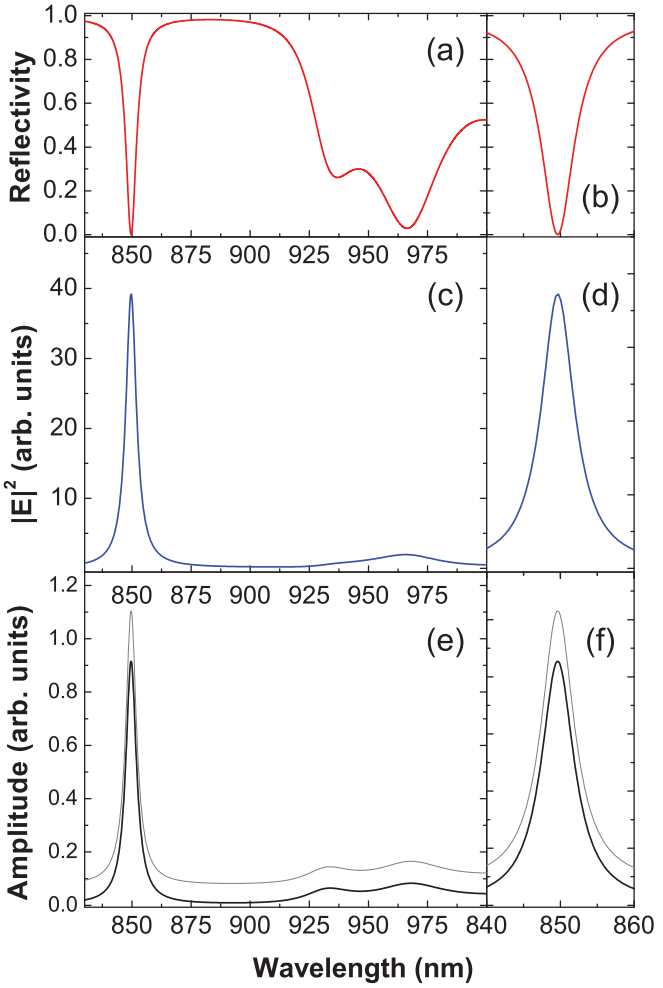

FIG. 4. (Color online) Coherent generation of zone center acoustic phonons. (a),(b) Optical reflectivity of the light resonator. (c),(d) The calculated electric field intensity in the center of the optical microcavity. (e),(f) Calculated intensity of the generated spectrum. In black (gray) a structure where the photoelastic constant is purely real (imaginary). Observe that the two curves present identical behaviors.

IV. COHERENT PHONON DETECTION

To study the detection process in an optical microcavity, independently of the generation mechanism, we assume a "white" phonon wave packet incident from the substrate side, and we compute the optical reflectivity as a function of the probe wavelength. To simulate the detection mechanism we consider that acoustic phonons produce a change in the index of refraction proportional to the strain (and to the photoelastic constant) in the superlattice materials. This change in the index of refraction induces a change in the optical reflectivity of the whole structure. The change in the index of refraction (n) induced by a phonon of frequency ω is calculated as

$$\Delta n(z,\omega) = \frac{\partial u(z,\omega)}{\partial z}\frac{p(z)}{2n_0}. \tag{7}$$

Taking into account the modified index of refraction defined as

$$n(z,\omega) = n_0(z) + \Delta n(z,\omega), \tag{8}$$

it is possible to calculate the perturbed reflectivity of the sample $|r(\omega)|^2$. Then, the variation in reflectivity as a function of the wavelength will be computed as

$$\Delta R(\lambda,\omega) = ||r_0(\lambda)|^2 - |r(\lambda,\omega)|^2|, \tag{9}$$

where $r_0(\lambda)$ ($r(\lambda)$) is the unperturbed (perturbed) reflectivity.

The detected spectrum of coherent phonons in a simple superlattice grown on a GaAs substrate is shown in Fig. 2(d). Two principal peaks (indicated with BS) can be observed, and are related to phonons with wave vector $q = 2k$, which are Raman active in backscattering geometry. Note that the peak that was observed in Fig. 2(c) is not present in this spectrum. In other words, the superlattice generation spectrum does not overlap its detection spectrum.[40,41] In spite of this mismatch, several experimental works reported the observation of the three peaks (two BS and one FS). This is due to a relaxation of the selection rules due to light absorption, finite size effects, excitonic resonances, and possible light backreflections.[41,42] However, in all these cases, the overlap between the generation and detection spectra is far from perfect. As was previously mentioned, the optical microcavity changes not only the intensity of the electric field within the spacer but also its spatial distribution, modifying also the detection selection rules. In Fig. 2(f) we show the calculated detection spectrum when the SL is embedded in the optical microcavity, with the laser tuned with the edge of the optical microcavity mode. It can be noted that three peaks are present, in coincidence with the generation spectrum shown in Fig. 2(e). In the next section we study this matching as a function of the laser wavelength.

In Fig. 5 we show the intensity map of the detected spectrum of the same superlattice embedded in the optical microcavity assuming a purely real photoelastic constant. Again, a white-spectrum phonon pulse is assumed to be incident from the substrate side. Darker regions represent higher detection amplitudes. In the top panel we include the calculated optical reflectivity of the microcavity and in the left panel the acoustic reflectivity (thick line) and a detection spectrum calculated for a probe wavelength $\lambda = 851.6$ nm corresponding to a maximum of the signal intensity (gray line). From the intensity map it can be noted that (i) there are two dark bands around 850 nm where the detected spectrum presents its maximum amplitude and a central band at 850 nm where the intensity is null; (ii) at these resonances there is an intense peak at 0.48 THz, corresponding to an acoustic excitation with $q = 0$ in addition to those expected at $q = 2k$ (0.45 and 0.53 GHz); (iii) the detected signal is negligible in the stop band; and (iv) between 920 and 1000 nm a series of weak signals can be observed associated with phonons with $q = 0$ and $q = 2k$, whose relative intensities vary with the probe wavelength.

The presence of two maxima around the optical cavity mode can be explained considering that, according to the proposed photoelastic model, acoustic phonons with frequency ω modulate the refraction index of the microcavity spacer. This variation induces a change in the reflectivity with the same frequency, which at first order of approximations can be associated with a displacement of the microcavity mode around the unperturbed position. In the considered detection model we evaluate this variation as a function of the laser wavelength. A differential change in the index of refraction (or equivalently a change in the spacer thickness) originates a differential change in the cavity mode position. This variation induces stronger changes in the reflectivity in spectral regions where the cavity presents the strongest variation in reflectivity. In other words, the optical mode center is insensitive to differential changes in the index of refraction, while in the mode edges, where the reflectivity presents the strongest variations, the system will have the maximum sensitivity. Taking this into account, a simple way to evaluate the sensitivity of the system is to calculate the derivative of the reflectivity with respect to the wavelength.

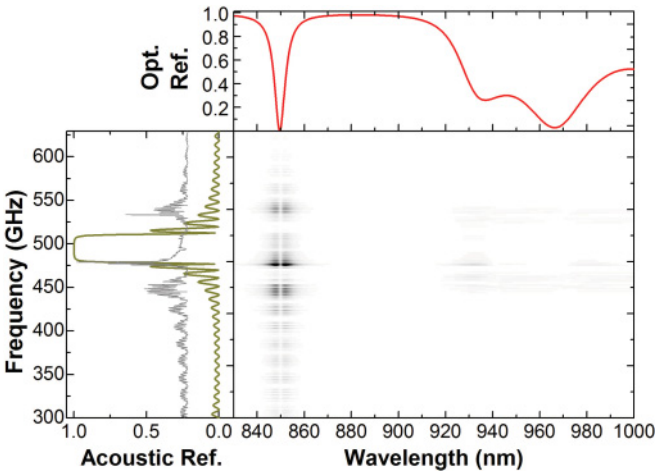

FIG. 5. (Color online) Calculated amplitude of the coherent detection spectrum as a function of the laser wavelength and the acoustic phonon frequency for a purely real photoelastic constant. (Top) Optical reflectivity of the sample. (Left) Acoustic reflectivity (thick line) and detection spectrum (gray thin line) calculated with a laser wavelength $\lambda = 851.6$ nm.

Figure 6 shows the optical reflectivity [panels (a) and (b)], the absolute value of the reflectivity derivative with respect to the wavelength [panels (c) and (d)], and the amplitude of the detected FS peak considering $p_{GaAs} = 250$ [panels (e) and (f), black curve] as a function of the laser wavelength. In panels (e) and (f) we also include in gray the amplitude of the detected FS peak considering $p_{GaAs} = 250i$, where i is the imaginary unit. Panels (b), (d), and (f) show a zoom around the optical microcavity mode. The amplitude of the detected signal (case p real) presents two maxima around the cavity mode and a zero at its center. It mimics the general behavior of the curve shown in panels c and d. On the contrary, the gray curve, corresponding to the imaginary photoelastic constant, presents three maxima instead of two in the cavity mode region. Moreover, in the region between 900 and 1000 nm it can be noted that each maximum of the gray curve corresponds to a minimum of the black curve and vice versa. By observing the two extreme cases (p being purely real or purely imaginary), it is clear that the response of the microcavity is strongly dependent on the nature of the photoelastic constants of the materials forming the spacer. We recall that in Fig. 4(e), the maximum of the generation spectra coincides with the center of the cavity mode, independently of the real or imaginary nature of p.

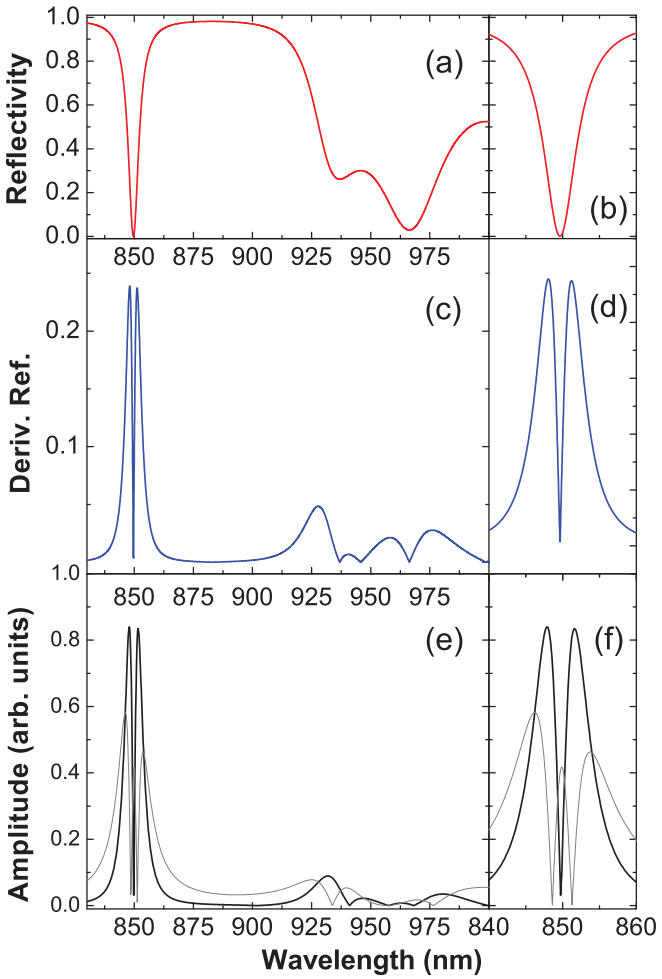

FIG. 6. (Color online) Coherent detection of zone center acoustic phonons when an acoustic pulse is assumed to be incident from the substrate side. (a),(b) Optical reflectivity of the light resonator. (c),(d) Calculated derivative of the optical reflectivity as a function of the wavelength. (e),(f) Calculated intensity of the detected spectrum. In black (gray) a structure where the photoelastic constant is purely real (imaginary). Observe that the two curves present different behaviors in the whole wavelength range.

In order to analyze the behavior of the microcavity sensitivity dependence with the photoelastic constant, in Fig. 7 we plot the amplitude of the FS mode in the detection spectrum as a function of the probe wavelength. The curves have been vertically shifted 0.2 units for clarity reasons. We take the photoelastic constant of the GaAs layers in the microcavity spacer to be equal to $250e^{i\pi t}$, with t taking the values 0, 1/4, and 1/2. The vertical lines indicate the cavity mode position and the maxima of the reflectivity derivative. In the case where the photoelastic constant is purely real two maxima can be observed, which coincide with the maxima of the derivative. In addition, when the laser is tuned with the cavity mode, there is an absolute zero; that is, no signal can be detected at 850 nm, independently of the intensity of the electromagnetic field inside the cavity. On the other extreme, when the photoelastic constant is purely imaginary, three maxima can be observed. The central maximum is practically located at the cavity mode center. There are two zeros limiting the central maximum.

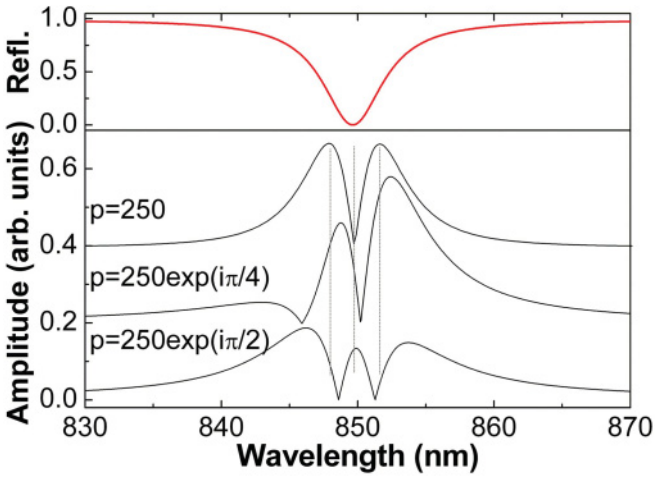

FIG. 7. (Color online) Influence of the real/imaginary nature of the photoelastic constant p in the coherent phonon detection process using optical microcavities. The curves have been vertically shifted for clarity reasons.

By changing the real/imaginary ratio it is possible to get a continuous variation of the position of the zeros and maxima. For the case $t = 1/4$ an asymmetric position of the zeros can be obtained. Moreover, since in this case there are two materials that form the optical spacer it is possible to tune the position of the zeros in the sensitivity (for example with one photoelastic constant real and the other one complex). Inversely, it would be possible to determine the photoelastic constants by properly determining the spectral response of the structure embedded in the optical microcavity.

V. MODIFICATION OF THE SELECTION RULES USING OPTICAL MICROCAVITIES

In this section we analyze the modification of the selection rules for both the generation and the detection of coherent acoustic phonons as a function of the tuning of the laser and microcavity mode. For the sake of simplicity we take all the generation and photoelastic constants as real numbers. Figure 8(b) [8(c)] shows the intensity of the generation [detection] spectrum for phonons of 498.7 GHz in black and 531.2 GHz in gray, with $q \approx 2k$ and $q \approx 0$, respectively. In panel (a) the calculated optical reflectivity is presented. To facilitate the comparison between the two cases, the curves have been normalized by the maximum value achieved in the region around the optical cavity mode. Between 880 and 1000 nm, a zoom of the curves is also shown.

In the case of the generation process [Fig. 8(b)], the two curves reach a maximum at the center of the optical microcavity mode. Between 880 and 1000 nm, the gray curve ($q \approx 0$) presents its maxima at the minima of the reflectivity. At those points there is a bigger optical density of states, and thus a partial amplification of the local electromagnetic field. The maxima of the black curve ($q \approx 2k$) are located approximately at the same positions. Note that in a superlattice without optical confinement, the generation is only effective for $q \approx 0$ and results essentially independent of the laser wavelength (neglecting excitonic resonances). For the detection process [Fig. 8(c)], in the region around the optical microcavity mode,

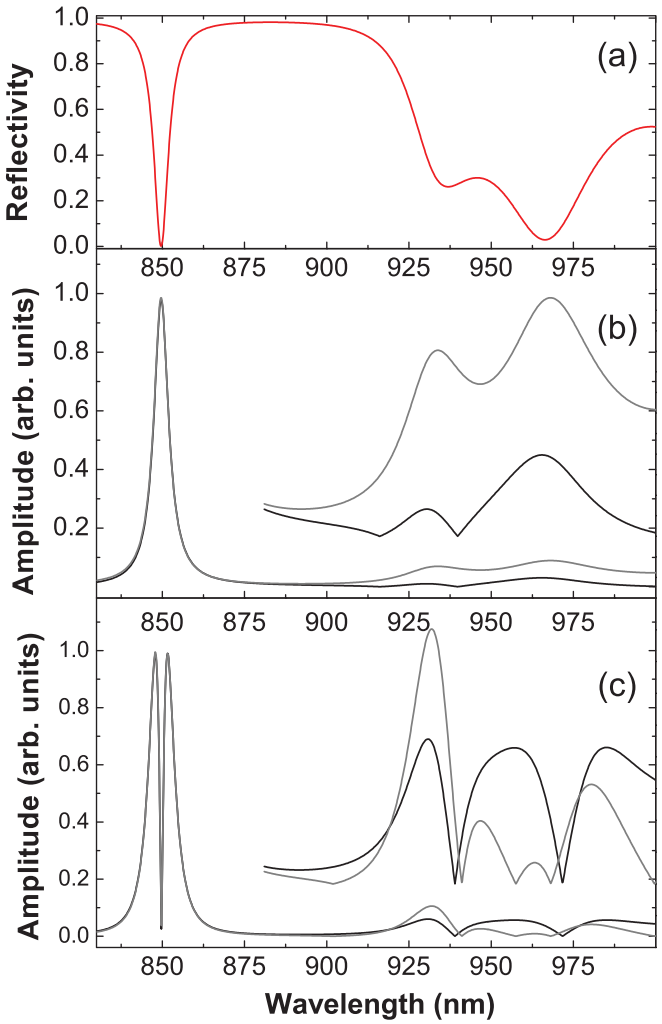

FIG. 8. (Color online) Selection rules for the coherent generation and detection of acoustic phonons. (a) Calculated optical reflectivity. (b) Generation spectral amplitude. (c) Detection spectral amplitude. The black (gray) curves correspond to a phonon with frequency 498.7 GHz (531.2 GHz) with $q \approx 2k$ ($q \approx 0$).

the curves present identical behaviors and reach two maxima at the mode edges. Between 880 and 1000 nm, the gray curve ($q \approx 0$) presents four zeros, while in the case of the black curve only two zeros can be identified. Observe that a superlattice without optical confinement only phonons with $q \approx 2k$ can be detected, and results, as in the case of generation, independent of the optical wavelength. This result implies that in a pump-probe experiment, with a laser wavelength set around the optical microcavity mode, the generated spectrum would be identical to the detected spectrum, thus obtaining an additional enhancement due to the cavity confinement.

It follows that the microcavity modifies not only the intensities of the signals, but also the selection rules for the generation-detection processes. The enhancement of the coherent phonon generation is proportional to the amplification of the electric field intensity. For the studied structure we obtained an amplification factor of ∼20 for the generation process of a phonon with $q \approx 0$, comparing the amplitude of the spectrum of a superlattice without and with optical microcavity. Note that this amplification is approximately half of the maximum amplification reached by the field intensity in the cavity (see Fig. 1). This can be explained by observing that the electric field is described as a *cosine* function, and thus the excitation results modulated along the optical spacer varying from the maximum intensity value (40 times the incident field) to a minimum reached at the node.

On the other hand, the enhancement of the detection process, considering real photoelastic constants, is given by the derivative of the reflectivity curve. The value of this derivative will be increased when the cavity finesse is increased. Comparing the detection signals calculated for the superlattice with and without optical confinement for a phonon with $q \approx 2k$, we obtained an enhancement factor of ∼80.

VI. DOUBLE OPTICAL ENHANCEMENT

In the previous sections we have observed that the maximum enhancement for the generation process takes place when the pump laser is perfectly tuned with the optical microcavity mode. On the contrary, when considering real photoelastic coefficients, the maximum enhancement of the detection is achieved at the points where the derivative of the reflectivity presents its maxima. In this section we analyze the total enhancement factors achieved when both conditions are fulfilled. We call this condition DOE and the total enhancement factor DOE factor. From the experimental point of view, the DOE can be reached by means of three methods: (i) using different wavelengths for the pump and probe beams; (ii) filtering the laser pulses in order to get different spectral components in each beam; or (iii) taking advantage of the microcavity light dispersion, and varying independently the angle of incidence of the pump and probe beams.[25]

To simulate the DOE condition we used a two-step process. First, we simulate the generation process under normal incidence with the laser wavelength tuned with the optical microcavity mode, as explained in Sec. III. Then the generated phonon spectrum is used as a seed to simulate the detection process, as explained in Sec. IV. In other words, the simulation of the detection does not consider a white incident phonon spectrum anymore, but the simulated one in the generation step. We used different wavelengths for both pump and probe. We select the probe wavelength to coincide with the maximum value of the reflectivity derivative, that is, corresponding to the method (i) above. The results are identical to what would be obtained by modeling the experiment with different angles of incidence for pump and probe beams to attain the same DOE condition [method (iii) above]. All the calculated intensities are normalized to the case of a identical SL grown on top of a simple GaAs substrate.

Figure 9(b) shows the calculated coherent phonon generation-detection spectrum under DOE in the optical SL embedded in the optical microcavity. Figure 9(a) shows the same simulation performed using the bare SL on top of a GaAs substrate. Note how the main features usually observed under backscattering and forward scattering geometries in Raman experiments (labeled as BS and FS, respectively) appear in both spectra. The finite size of the sample allows the observation of the three peaks in the case of the bare superlattice, in spite of the weak overlapping between the generation and detection spectra. The enhancement factor

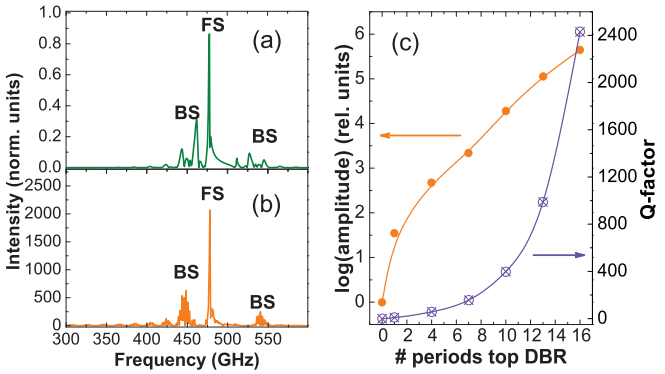

FIG. 9. (Color online) Coherent phonon generation and detection under DOE condition. (a) Simulated spectrum of a pump-probe experiment on a bare SL on top of a GaAs substrate. (b) Simulated spectrum of the same SL embedded in the studied optical microcavity under the DOE condition. BS and FS indicate acoustic modes observed under backscattering and forward-scattering geometries in Raman experiments. (c) Enhancement factor under DOE (solid circles) and Q factor of the optical microcavity (crossed open circles) as a function of the number of periods forming the DBRs.

achieved with the considered optical microcavity was 2300. The high-frequency oscillations in Fig. 9(b) are related to the additional acoustic modulation introduced by the optical DBRs. In Fig. 9(c) we compare the efficiency of different optical microcavities. The microcavities are formed by a top (bottom) DBR of N ($N + 3$) periods. The full circles correspond to the logarithm of the achieved amplitude. For a microcavity with 16 (19) periods in the top (bottom) DBR the signal is almost six orders of magnitude bigger than in the case of the bare SL. With crossed empty circles we plot the associated Q factor of the microcavity, being the highest around 2400. Cavity Q factors in these range are standard for planar semiconductor microcavities grown with molecular beam epitaxy.

VII. DISCUSSION AND CONCLUSIONS

We have studied how a planar optical microcavity modifies the efficiency and selection rules of the generation and detection of coherent acoustic phonons. We observed that around the optical cavity mode, peaks associated to $q \sim 0$ and $q \sim 2k$ become active for both the generation and the detection processes. So, under optical confinement, the phonons that modulate the optical reflectivity are exactly the same phonons that were created, enhancing the signals with respect to standard experiments. Analyzing how the generation is enhanced by the presence of the optical microcavity, the generated signal reaches its maximum when the excitation laser is exactly tuned with the optical microcavity mode. This behavior is not affected by the real/imaginary nature of the used generation constants. When assuming real photoelastic constants, the coherent phonon detected signal, on the contrary, reaches a zero when the laser is exactly tuned with the optical microcavity mode. There are two maxima in the detection efficiency that are located at the points where the reflectivity derivative presents its extreme values (either positive or negative). Thus, for a single laser wavelength and under normal incidence, both generation and detection cannot be simultaneously optimized.

We have observed that the detection sensitivity strongly depends on the real/imaginary nature of the photoelastic constants in the spacer. Particularly, the location of the zeros in the detection spectrum is determined by the real/imaginary parts ratio. Thus, optical microcavities could be used for the determination of photoelastic constants in novel structures and materials. However, it must be noted that in the case of high-frequency phonons, laser pulses of 80 fs or less are used. This implies that the resolution to obtain photoelastic constants as a function of the laser energy is limited.

In order to maximize the pump-probe signal, it is then necessary to tune the maximum of the generated spectrum (at the center of the optical cavity mode) and that of the detected spectrum (at the edges of the optical cavity mode). We have introduced the concept of DOE, obtaining a total enhancement factor 2300 for an optical microcavity with a Q factor of $\sim$160. This value is good enough to apply this measurement configuration to systems where the photoelastic constants are too small. Maris *et al.*[24] have started working on this subject implementing an external microcavity to amplify signals in metals and water-based systems. Using cavities with higher Q factors, enhancements of more than six orders of magnitude can be envisaged. The discussed results open the path to address novel problems and applications in nanophononics including the study of phonon stimulation, nonlinear effects and efficient phonon-imaging systems.

ACKNOWLEDGMENTS

This work is part of the International French Argentinian Nanoscience Laboratory, LIFAN.

*kimura@cab.cnea.gov.ar.

[1]N. D. Lanzillotti-Kimura, A. Fainstein, A. Lemaitre, and B. Jusserand, Appl. Phys. Lett. **88**, 083113 (2006).

[2]N. D. Lanzillotti-Kimura, A. Fainstein, B. Jusserand, A. Lemaitre, O. Mauguin, and L. Largeau, Phys. Rev. B **76**, 174301 (2007).

[3]N. D. Lanzillotti-Kimura, B. Perrin, A. Fainstein, B. Jusserand, and A. Lemaitre, Appl. Phys. Lett. **96**, 053101 (2010).

[4]Kung-Hsuan Lin, Chih-Ming Lai, Chang-Chi Pan, Jen Inn Chyi, Jin-Wei Shi, Shih-Ze Sun, Chieh-Feng Chang, and Chi-Kuang Sun, Nat. Nanotech. **2**, 704 (2007).

[5]A. Huynh, N. D. Lanzillotti-Kimura, B. Jusserand, B. Perrin, A. Fainstein, M. F. Pascual-Winter, E. Perónne, and A. Lemaître, Phys. Rev. Lett. **97**, 115502 (2006).

[6]Ke-Qiu Chen, Xue-Hua Wang, and B. Y. Gu, Phys. Rev. B **61**, 12075 (2000).

[7]M. Trigo, A. Bruchhausen, A. Fainstein, B. Jusserand, and V. Thierry-Mieg, Phys. Rev. Lett. **89**, 227402 (2002).

[8]N. D. Lanzillotti-Kimura, A. Fainstein, C. A. Balseiro, and B. Jusserand, Phys. Rev. B **75**, 024301 (2007).

[9]N. D. Lanzillotti-Kimura, A. Fainstein, A. Huynh, B. Perrin, B. Jusserand, A. Miard, and A. Lemaitre, Phys. Rev. Lett. **99**, 217405 (2007).
[10]N. D. Lanzillotti-Kimura, A. Fainstein, B. Perrin, B. Jusserand, A. Soukiassian, X. X. Xi, and D. G. Schlom, Phys. Rev. Lett. **104**, 187402 (2010).
[11]J. Groenen, F. Poinsotte, A. Zwick, C. M. Sotomayor Torres, M. Prunnila, and J. Ahopelto, Phys. Rev. B **77**, 045420 (2008).
[12]N. Lou, J. Groenen, G. Benassayag, and A. Zwick, Appl. Phys. Lett. **97**, 141908 (2010).
[13]D. Moss, A. V. Akimov, O. Makarovsky, R. P. Campion, C. T. Foxon, L. Eaves, A. J. Kent, and B. A. Glavin, Phys. Rev. B **80**, 113306 (2009).
[14]M. T. Greenaway, A. G. Balanov, D. Fowler, A. J. Kent, and T. M. Fromhold, Phys. Rev. B **81**, 235313 (2010).
[15]N. D. Lanzillotti-Kimura, A. Fainstein, B. Jusserand, and A. Lemaitre, Phys. Rev. B **79**, 035404 (2009).
[16]P. Lacharmoise, A. Fainstein, B. Jusserand, and V. Thierry-Mieg, Appl. Phys. Lett. **84**, 3274 (2004).
[17]B. Jusserand and M. Cardona, in *Light Scattering in Solids V*, edited by M. Cardona and G. Güntherodt (Springer, Heidelberg, 1989).
[18]C. Thomsen, H. T. Grahn, H. J. Maris, and J. Tauc, Phys. Rev. B **34**, 4129 (1986).
[19]P. Babilotte, P. Ruello, D. Mounier, T. Pezeril, G. Vaudel, M. Edely, J-M. Breteau, V. Gusev, and K. Blary, Phys. Rev. B **81**, 245207 (2010).
[20]O. Matsuda and O. B. Wright, J. Opt. Soc. Am. B **19**, 3028 (2002).
[21]A. Fainstein, B. Jusserand, and V. Thierry-Mieg, Phys. Rev. Lett. **75**, 3764 (1995).
[22]A. Fainstein, B. Jusserand, and V. Thierry-Mieg, Phys. Rev. B **53**, R13287 (1996).
[23]A. Fainstein and Bernard Jusserand, Phys. Rev. B **57**, 2402 (1998).
[24]Y. Li, Q. Miao, A. V. Nurmikko, and H. J. Maris, J. Appl. Phys. **105**, 083516 (2009).
[25]N. D. Lanzillotti-Kimura, A. Fainstein, B. Perrin, B. Jusserand, L. Largeau, O. Mauguin, and A. Lemaitre, Phys. Rev. B **83**, 201103 (2011).
[26]A. Huynh, B. Perrin, N. D. Lanzillotti-Kimura, B. Jusserand, A. Fainstein, and A. Lemaître, Phys. Rev. B **78**, 233302 (2008).
[27]A. Fainstein and B. Jusserand, Light Scattering Solids IX: Novel Mater. Tech. **108**, 17 (2007).
[28]B. Sermage, S. Long, I. Abram, J. Y. Marzin, J. Bloch, R. Planel, and V. Thierry-Mieg, Phys. Rev. B **53**, 16516 (1996).
[29]M. S. Skolnick, T. A. Fisher, and D. M. Whittaker, Semicond. Sci. Technol. **13**, 645 (1998).
[30]J. Kasprzak, M. Richard, S. Kundermann, A. Basas, P. Jeambrun, J. M. J. Keeling, F. M. Marchetti, M. H. Szymanska, R. Andre, J. L. Staehli, V. Savona, P. B. Littlewood, B. Deveaud, and L. S. Dang, Nature (London) **443**, 409 (2006).
[31]Hui Deng, D. Press, Stephan Gotzinger, Glenn S. Solomon, Rudolf Hey, Klaus H. Ploog, and Yoshihisa Yamamoto, Phys. Rev. Lett. **97**, 146402 (2006).
[32]Guillaume Malpuech, Aldo Di Carlo, Alexey Kavokin, Jeremy J. Baumberg, Marian Zaprescu, and Paolo Lugli, Appl. Phys. Lett. **81**, 412 (2002).
[33]G. Malpuech, A. Kavokin, A. Di Carlo, and J. J. Baumberg, Phys. Rev. B **65**, 153310 (2002).
[34]K. Mizoguchi, M. Hase, S. Nakashima, and M. Nakayama, Phys. Rev. B **60**, 8262 (1999).
[35]N. D. Lanzillotti-Kimura, A. Fainstein, B. Perrin, B. Jusserand, O. Mauguin, L. Largeau, and A. Lemaitre, Phys. Rev. Lett. **104**, 197402 (2010).
[36]R. P. Beardsley, A. V. Akimov, M. Henini, and A. J. Kent, Phys. Rev. Lett. **104**, 085501 (2010).
[37]Ivan S. Grudinin, Hansuek Lee, O. Painter, and Kerry J. Vahala, Phys. Rev. Lett. **104**, 083901 (2010).
[38]S. Adachi, J. Appl. Phys. **58**, R1 (1985).
[39]A. Bartels, T. Dekorsy, H. Kurz, and K. Kohler, Appl. Phys. Lett. **72**, 2844 (1998).
[40]M. Trigo, T. A. Eckhause, J. K. Wahlstrand, R. Merlin, M. Reason, and R. S. Goldman, Appl. Phys. Lett. **91**, 023115 (2007).
[41]M. F. Pascual Winter, A. Fainstein, B. Jusserand, B. Perrin, and A. Lemaître, Appl. Phys. Lett. **94**, 103103 (2009).
[42]Albrecht Bartels, Thomas Dekorsy, Heinrich Kurz, and Klaus Kohler, Phys. Rev. Lett. **82**, 1044 (1999).